

## Theoretical study of high-density phases of covalent semiconductors. I. *Ab initio* treatment

J. Crain, S. J. Clark, G. J. Ackland, M. C. Payne,\* V. Milman,\* P. D. Hatton,  
and B. J. Reid

*Department of Physics, The University of Edinburgh, Mayfield Road, Edinburgh, Scotland EH9 3JZ, United Kingdom*  
(Received 14 May 1993)

We present detailed calculations using the total-energy pseudopotential method in the local-density approximation of the relative stability and pressure-induced behavior of complex tetrahedrally bonded structures formed metastably in silicon and germanium by depressurization from their metallic phases. The corresponding structures in carbon are also investigated. These calculations present direct atomistic relaxation of BC8 under the influence of Hellmann-Feynman forces and, to our knowledge, the first calculations on the ST12 structure using any form of relaxation. We also present evidence to show that in both Si and Ge the BC8 and ST12 structures are covalently bonded, while the equivalent structures in carbon cannot support such covalent bonding.

### I. INTRODUCTION

It is somewhat surprising that after many years of study the polymorphism of the elements silicon and germanium is still unresolved. This is due to the extreme complexity and to the presence of metastable phases. Silicon displays at least 11 different crystalline phases at pressures up to 248 GPa<sup>1</sup> some of which can be recovered as metastable phases at atmospheric pressure. In germanium transitions to the  $\beta$ -Sn structure, hcp and dhcp have been observed up to 125 GPa.<sup>2</sup> In addition, metastable phases can be obtained either by pressure decrease from the metallic phases<sup>3</sup> or by chemical leaching of lithium from Li<sub>7</sub>Ge<sub>12</sub>.<sup>4</sup> Very recently, it has been found that small regions of metallic silicon can be obtained by nanoindentation.<sup>5</sup>

For carbon it is impossible to perform experiments on phases with higher density than diamond because of the huge pressures involved. Indeed, in most pressure experiments carbon diamond-anvil cells are used to produce the required pressure. In view of the existence of a covalently bonded diamond phase, it seems reasonable to investigate whether the phase diagram may be similar to Si and Ge. Calculations of metallic phases in carbon do, however, suggest that these are not significantly denser than diamond.<sup>6</sup>

Silicon has been an ideal material for combining experiment and total energy calculations. In their groundbreaking paper, Yin and Cohen<sup>7</sup> predicted that the  $\beta$ -Sn phase would transform to hcp at 43 GPa. In the search for this transition, experimental results revealed another phase, simple hexagonal, which Yin and Cohen had not examined. On repeating the calculation the stability of the simple hexagonal structure was confirmed. Similar calculations have been carried out in germanium and carbon, examining both stable and metastable phases.<sup>8,6,9</sup>

*Ab initio* total-energy calculations are sufficiently accurate to have a predictive capability, and certainly their success in reproducing many experimental features of condensed matter is impressive. As illustrated by the

above example, however, it is often important to know what to expect before beginning the calculation, so that all reasonable possibilities are examined. A further complication is that the rate at which first-order phase transitions occur varies enormously, so that the lifetimes of some metastable phases are essentially infinite because of the large kinetic barrier to transition. Since the transition path is seldom known, the lifetime of metastable phases cannot be readily calculated.

Metastable phases of the group-IV elements have long been of great practical and theoretical interest. The hardness of diamond has been utilized since ancient times, while more recently amorphous silicon has found numerous uses. With pressure treatment it is also possible to create high-density phases of Si and Ge which are long-lived under normal conditions. These complex structures have been shown to be useful models in exploring the effect of increasing short-range disorder on optical properties and have provided a vital insight into the nature of the amorphous phase of these materials.<sup>10,11</sup> We have carried out a thorough study of these metastable phases: BC8 and ST12, both in silicon and germanium where they have been observed experimentally, and in carbon. In addition to revealing the structural stability and nature of the bonding, the results will be a useful guide in determining the degree to which simple empirical models can account for the structural trends. This issue will be described in detail in the related paper, Ref. 12 (hereafter referred to as Paper II).

Silicon BC8 and germanium ST12 phases are reasonably easy to synthesize. Under a pressure of about 12.5 GPa, diamond Si transforms to the  $\beta$ -Sn phase.<sup>13</sup> This is a massively first-order phase transition in which the structure transforms from fourfold to sixfold coordination and the material itself transforms from semiconductor to metal. There is no easy kinetic path for this transition, and on depressurization there is considerable hysteresis. Eventually, at about 8 GPa the  $\beta$ -Sn phase transforms back, not to diamond, but to the BC8 phase.<sup>14</sup> The lifetime of BC8 silicon under ambient conditions seems to be indefinite.

The nature and number of metastable phases formed on depressurization appear to depend upon whether the original sample is amorphous or crystalline, the temperature, and the rate of depressurization. Slow decompression from crystalline ( $\beta$ -Sn phase) Si at ambient temperature gives a mixture of amorphous silicon, diamond, and BC8.<sup>15</sup> Upon rapid release of pressure from the metallic state, two tetragonal phases have been obtained.<sup>14</sup> It appears that, once converted to any metallic form by application of pressure, silicon reverts to BC8 and the diamond form cannot be recovered, even by heat treatment and recrystallization when the Lonsdaleite structure (hexagonal diamond) is formed.<sup>16</sup>

The polymorphism of germanium is similarly complex. Pressure increase from the cubic diamond structure results in the  $\beta$ -Sn structure at 10.6 GPa.<sup>17</sup> Slow pressure decrease results in the formation of diamond and ST12 germanium<sup>18</sup> at 7.6 GPa. A metastable form of germanium in the BC8 structure has also been observed on pressure decrease.<sup>19,20</sup>

In carbon no phases with higher density than diamond have been made.

The discovery of the BC8 phase, its identification as a semimetal (with resistivity about a thousand times lower than the semiconducting diamond form and a hundred times higher than the  $\beta$ -Sn form), and the crystallographic structural solution have been reported previously.<sup>21–26</sup> There have also been some total energy calculations on the BC8 phase in silicon,<sup>27,6,9</sup> and in carbon<sup>6,9</sup> where it has been predicted to be stable over a range of very high pressures. This has not been experimentally verified, and for obvious reasons is impossible with conventional diamond-anvil pressure cells.

In this paper we present complete total-energy pseudopotential calculations of the behavior of BC8 carbon, silicon, and germanium under pressure, including direct atomic relaxation of the atomic positions using the Hellmann-Feynman forces. We also report a similarly thorough study of these elements in the ST12 structure, in which we relax the  $c/a$  ratio of the tetragonal unit cell in addition to all the atomic positional parameters. The number of free parameters in this case is sufficiently large that a relaxed solution of the ST12 structure has not previously been carried out to our knowledge.

The relaxed structures enable us to compare the different behavior of silicon and germanium, whose overall phase diagrams are similar, and carbon, which exhibits similar, covalent bonding. In Paper II, we shall examine the free energy of the two phases and show that ST12 is expected to be preferred at high temperatures.

The organization of the paper is as follows. In Sec. II the details of the computational techniques will be described. In Sec. III the crystallographic data on the known metastable structures of group-IV semiconductors will be discussed with an emphasis on the types of distortions found in each structure and the possible routes of transition between them. This will be followed in Sec. IV by the results of density-functional total-energy calculations on fully relaxed structures of Si, Ge, and C. A detailed study of the response of the internal structure to compression will be presented for each of the three ele-

ments in Sec. V and in Sec. VI the nature of the bonding is explored.

## II. TOTAL-ENERGY CALCULATIONS

This work was carried out using codes developed at Edinburgh and Cambridge Universities (CASTEP and CETEP). These codes use the Car-Parrinello first-principles molecular-dynamics method,<sup>28</sup> of which full details and test results have been published elsewhere.<sup>29</sup> The program solves for the electronic charge density using a density-functional framework<sup>30</sup> within the local density approximation to exchange and correlation.<sup>31,32</sup> Norm-conserving, nonlocal, Kleinman-Bylander pseudopotentials<sup>33</sup> generated using the Kerker method<sup>34</sup> are used. The electronic wave functions are expanded in a plane-wave basis set with periodic boundary conditions, and different runs are done with the same plane wave energy cutoff of 250 eV for silicon and germanium and 408 eV for carbon. The higher value is required to ensure energy difference convergence for carbon because of the greater depth of the pseudopotential. This in turn arises because the  $2p$ -character valence orbitals are not kept away from the nucleus by orthogonalization with other  $p$  orbitals.

The electronic degrees of freedom are relaxed using a conjugate-gradients routine modified to conserve orthonormality of the one-electron wave functions.<sup>29</sup> Electronic relaxation continues until the Hellmann-Feynman forces have converged to three significant figures, and then the ions are moved using a conjugate-gradients algorithm. The ions are allowed to relax until the forces are below  $0.001\text{eV}/\text{\AA}$ . The unit cell for each calculation is not changed during a run, and because the plane-wave basis set is not localized on an atom there are no Pulay<sup>35</sup> forces arising from changes in the basis set while the atoms relax.

For silicon and carbon in diamond, ST12, and BC8 phases we used four special  $k$  points<sup>36</sup> at which the band structure was sampled. The same four  $k$ -point set was found to be insufficient to converge the very small ST12-diamond energy difference in germanium. Several sets of  $k$  points were tested and a set of ten was found to be sufficient. The complete pressure-dependent band structures will be presented elsewhere.<sup>11</sup> It also is possible that the frozen-core approximation for the germanium  $3d$  electrons may not be entirely justified and a full-potential treatment of these structures would therefore be necessary to explore this. The combination of cutoff and  $k$ -point sampling gives us total energies converged only to about 0.1 eV (four significant figures); however, the physically significant quantities, the total-energy differences between energy-volume curve minima, are converged to better than 0.01 eV, about half of which is attributable to differences between curve-fitting schemes (Murnaghan vs polynomial). In germanium the additional sampling gives still better convergence.

## III. INTERNAL STRUCTURE OF BC8 AND ST12

Diffraction evidence suggests that the postrecovered form of silicon has body-centered cubic symmetry with

16 atoms in the cubic unit cell and a lattice parameter of 6.64 Å. The space group of the structure is  $Ia\bar{3}T_h^7$ . The structure is then fully specified by a single lattice parameter and a single positional parameter  $x$  which has been experimentally reported<sup>37</sup> as being approximately  $0.1003 \pm 0.0008$  in silicon. A projection of the BC8 structure is shown in Fig. 1. The structure is based on tetrahedrally coordinated atoms, but with a rather more efficient packing than in diamond. This efficiency leads to a higher-density structure (hence favored at high pressures) at the expense of small distortions from the diamond bond length but with an appreciable change in the tetrahedral angle relative to the diamond structure. The distortions can be described by the existence of two bond lengths ( $R_A$  and  $R_B$ ) and two bond angles ( $\Theta_{AB}$  and  $\Theta_{BB}$ ). It is possible to choose special values of  $x$  to satisfy either  $R_A=R_B$  or  $\Theta_{AB} = \Theta_{BB}$  but in practice the observed values ( $R_A=2.30$  Å,  $R_B=2.39$  Å,  $\Theta_{AB} = 117.9^\circ$ , and  $\Theta_{BB} = 99.2^\circ$ )<sup>37</sup> seem to be a compromise between the two. All atoms are equivalent, and the structure contains only evenfold rings, the smallest being sixfold, as with diamond. Although BC8 exhibits a density some 10% higher than diamond, the  $B$  bond lengths are slightly larger.

The relations connecting bond lengths and the internal parameter  $x$  are as follows:

$$R_A/a_0 = 2\sqrt{3}x, \quad (1)$$

$$R_B/a_0 = \sqrt{8x^2 - 2x + 0.25}, \quad (2)$$

$$R_5/a_0 = \sqrt{3}(0.5 - 2x), \quad (3)$$

where  $R_A$  and  $R_B$  are the bond lengths of the  $A$  and  $B$  bonds, while  $R_5$  is the length of the nearest nonbonded neighbor and  $a_0$  is the lattice parameter (see Fig 1). The two bond angles also depend on  $x$  via the following relations:

$$\Theta_{AB} = \cos^{-1} \frac{(8x - 1)}{\sqrt{96x^2 - 24x + 3}}, \quad (4)$$

$$\Theta_{BB} = \cos^{-1} \frac{(4x^2 - x)}{8x^2 - 2x + 0.25}, \quad (5)$$

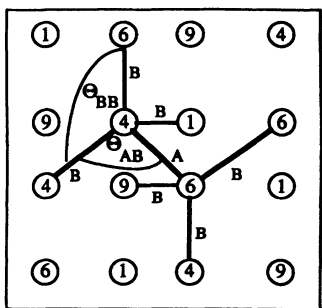


FIG. 1. Projection of the structure of BC8 on (001). Elevations (in  $a_0/10$ ) are given by the numbers inside the circles (Ref. 37).  $A$  and  $B$  label the two distinct bonds.

which allow a perfect tetrahedral angle at  $x = (5 - \sqrt{5})/40$ . This is never realized in atomic systems because it would require the  $A$  bond to be only 62% as long as the  $B$  bond. These expressions are useful because they show that the bond angles become less ideal with increasing  $x$ . Other values of  $x$  having interesting structural consequences are  $x = \frac{1}{8}$  where the structure becomes a threefold-coordinated layer structure with graphitic layers of type- $B$  bonds, and  $x \rightarrow \frac{1}{2} - x$  which is a transformation which leaves the structure unchanged. Thus increasing  $x$  can be regarded as a “magic internal strain”<sup>38</sup> similar to the so-called magic strains used to generate the BCT5 structure proposed as a high-pressure phase of silicon.<sup>39</sup> Symmetry also dictates that if it were possible to form a compound analogue of BC8 (from III-V or II-VI semiconductors) an increase in  $x$  would be the piezoelectric strain corresponding to the major axis of the polarizability tensor.

The postrecovered form of germanium, ST12, is more complex and its relaxation has not previously been tackled by *ab initio* calculations. A projection of the ST12 structure is shown in Fig. 2. Like BC8 it is based on tetrahedrally coordinated atoms packed in such a way as to increase the density to 10% above diamond. Crystallographic solution<sup>23</sup> of this phase cites it as having a simple tetragonal unit cell with 12 atoms. The structure would appear to be optically active, since it has left- and right-handed forms, although there has not yet apparently been any experiment done to examine this, presumably because of the difficulty in obtaining suitable single crystals. The space group is  $P4_32_12(D_8^4)$  or its enantiomorph. The fully relaxed structure can be defined by two lattice parameters and four atomic positional parameters.

In ST12 there are two distinct atomic environments, which leads to some rather complicated topological substructures. Four of the 12 atoms are in environment  $a$ , and the remaining eight in  $b$ . The  $b$  type can be viewed as forming spiral chains along the unique axis, while the  $a$  atoms bridge different spirals. All the spirals rotate the same way, giving the structure a well-defined helicity as noted above. Although the atoms are still fourfold coordinated, there are now five- and seven-membered rings, and the variation in bond angles (ranging from  $87^\circ$  to

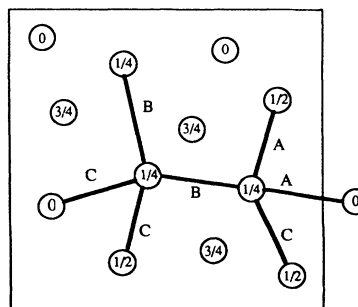


FIG. 2. Projection of the structure of ST12 on (001). Elevations (in fractional coordinates) are given by the numbers inside the circles (Ref. 37).  $A$ ,  $B$ , and  $C$  label the three distinct bonds.

130°) is greater than in BC8, but the bond lengths are clustered more closely around the value found in diamond. In Paper II we show that the stability of ST12 against BC8 rests in the compromise between equalizing bond lengths at the expense of increasing bond-angle distortions. ST12 occurs when the bond angles are relatively easier to distort.

#### IV. TOTAL ENERGIES

##### A. Silicon and germanium

Graphs of Murnaghan-equation fits to energy against volume for silicon and germanium in the ST12, BC8, and diamond phases are shown in Figs. 3(a) and (b). The ini-

tial unit-cell dimensions and internal structural parameters for ST12 were obtained from the empirical calculations described in Paper II. These graphs show that in each case the relaxed structures are unstable with respect to diamond at low pressures.

To obtain the curve for ST12 under hydrostatic pressure it was necessary to perform several series of calculations at several different  $c/a$  ratios, and to construct Fig. 4 which is a contour plot of the energy against volume and  $c/a$ . The hydrostatic curve is then the lowest value of the projection of this surface onto the volume axis. Figure 5 shows the variation of  $c/a$  with volume under hydrostatic pressure.

In silicon there is no intercept between the diamond- $\beta$ -Sn common tangent<sup>7</sup> and BC8 or ST12 curves,

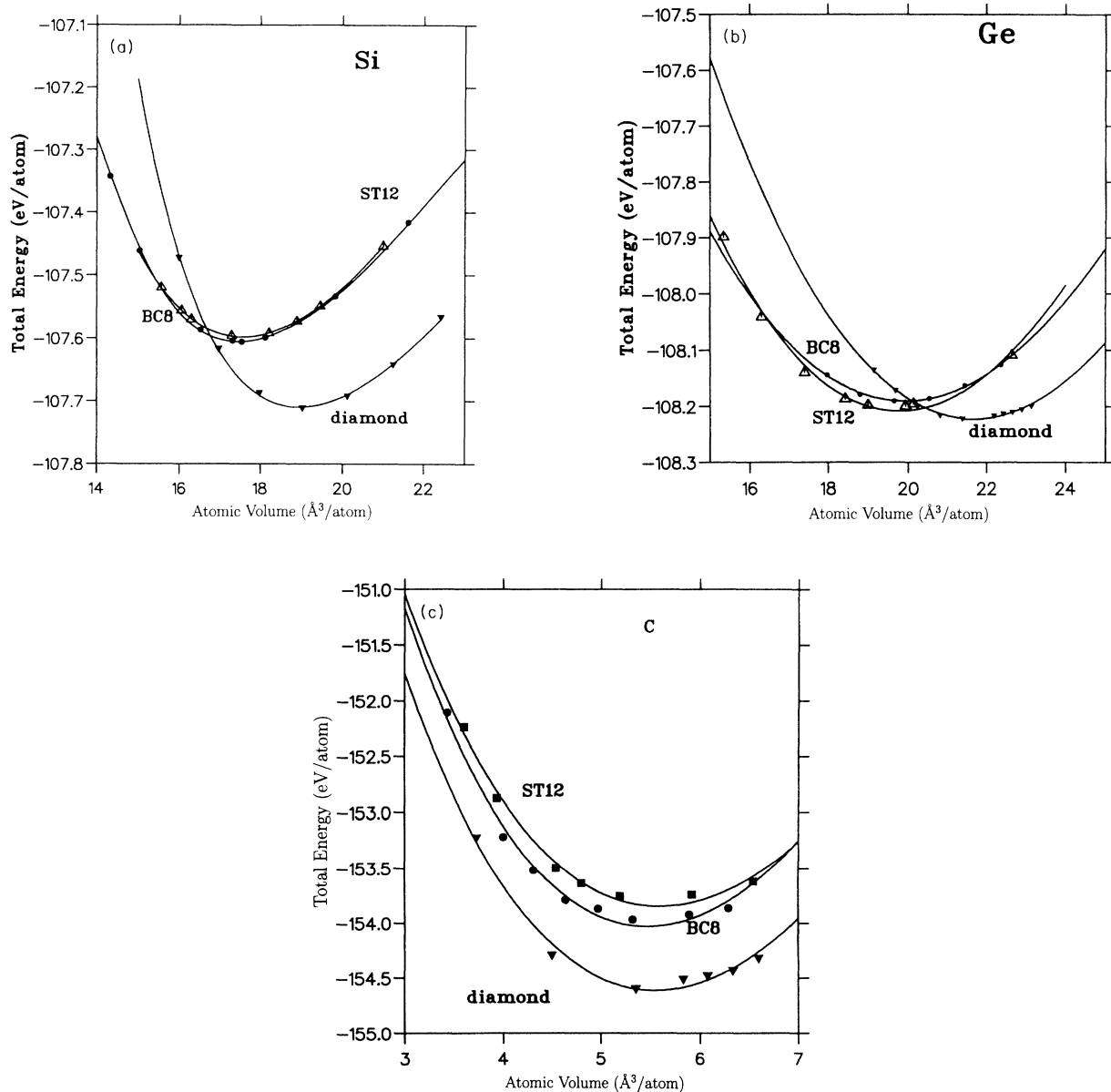


FIG. 3. Graphs of energy against volume for fully relaxed diamond, BC8, and ST12 structures in (a) silicon, (b) germanium, and (c) carbon.

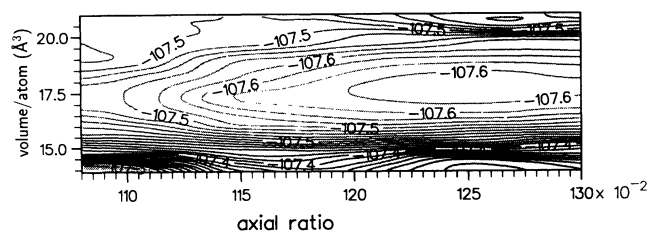


FIG. 4. Contour plot of cohesive energy against  $c/a$  ratio and atomic volume for ST12 structure in silicon.

from which we deduce that these phases are at best metastable. The common-tangent construction can also be used to predict the  $\beta$ -Sn  $\rightarrow$  BC8 transition pressure using previously published  $\beta$ -Sn data.<sup>7</sup> From these graphs we predict a transition pressure of only 11 GPa for silicon from the diamond structure to BC8. This is lower than the observed pressure for the diamond  $\rightarrow$   $\beta$ -Sn transition. This experimental value is above the theoretical value because of hysteresis effects resulting from the absence of an easy transition mechanism. The theoretical diamond  $\rightarrow$  BC8 transition pressure is greater than the calculated diamond  $\rightarrow$   $\beta$ -Sn pressure (9 GPa).<sup>6</sup> The calculated pressure between  $\beta$ -Sn and BC8 is 8 GPa (calculated according to  $\beta$ -Sn data from Ref. 6) in good agreement with depressurization experiments and suggestive of a relatively easy transition path.

In germanium the broad picture is similar but with ST12 being stable at intermediate pressure. The contour plot of energy against  $c/a$  and volume and the variation of  $c/a$  with volume for germanium ST12 are similar to those of silicon shown in Figs. 4 and 5. Unlike silicon, the common tangent between  $\beta$ -Sn and diamond cuts the ST12 curve, implying that for a range of pres-

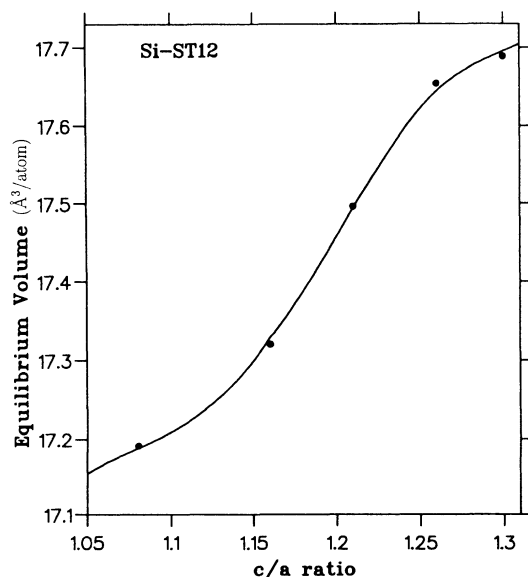


FIG. 5. Graph showing the variation of  $c/a$  in the ST12 structure as a function of volume.

ures ST12 is the stable structure. This result appears to contradict the observation of the first transition being to  $\beta$ -Sn. However, given the long experimental lifetime of the ST12 phase at ambient pressure,<sup>37,19</sup> it is clear that no easy diamond  $\rightarrow$  ST12 transformation path exists, and it is therefore likely that before the kinetic barrier can be overcome, the experimental pressure has been raised to that at which  $\beta$ -Sn is stable. Thus the only way to make ST12 germanium is via the  $\beta$ -Sn phase. It may even be that the retransformation from  $\beta$ -Sn to BC8 is easier than to ST12 because both structures have even-fold rings, such that BC8 may be formed as a precursor structure at low temperatures.

For all phases, the calculated results for the equilibrium structural parameters are in good agreement with those reported in previous studies. The lattice parameters and bulk moduli as determined by fits to a Murnaghan equation of state are given in Table I. As is usual in local-density-approximation (LDA) calculations, the lattice parameters are underestimated by about 2% (except for diamond germanium where the underestimate is only 0.5%). This means that we expect the bulk moduli to be overestimated; where experimental data exist this is indeed the case,  $B_0$  being overestimated by up to 8%.

Determination of the equilibrium axial ratio in both ST12-Si and ST12-Ge is crucial for accurate determination of energy differences in these phases. This is because it is found that the ST12 total energy for both materials varies by several tens of meV's over a  $c/a$  ratio range of 1.1–1.3. For the case of germanium the equilibrium axial ratio occurs at 1.24, which represents a 6% overestimate of the experimental value.<sup>19,37</sup> The calculated values for the relaxed atomic positional parameters, which are also sensitive to the  $c/a$  ratio, are discussed in more detail in the following section.

TABLE I. Calculated structural properties of silicon, germanium, and carbon in the diamond, BC8, and ST12 structures as determined from density-functional pseudopotential calculations. The units for the bulk modulus are  $\text{eV}/\text{\AA}^3$  and its pressure derivative is dimensionless.

Structure	$B_0$	Carbon		
		$B'_0$	$V_0$	$\frac{c}{a}$
		( $\text{\AA}^3/\text{atom}$ )		
Diamond	2.61	4.22	5.41	-
BC8	2.19	3.56	5.47	-
ST12	2.19	3.76	5.53	1.30
Silicon				
Diamond	0.6625	5.46	19.03	-
BC8	0.5890	5.54	17.48	-
ST12	0.5820	3.47	17.65	1.26
ST12	0.5660	3.67	17.57	Hydrostatic estimate
Germanium				
Diamond	0.479	5.9	22.46	-
BC8	0.476	4.2	19.78	-
ST12	0.454	4.0	19.47	1.20
ST12	0.444	3.9	19.65	1.25

The Murnaghan equation of state assumes a linear pressure dependence of the bulk modulus. The pressure derivative of the bulk modulus,  $B' = dB_0/dP$ , is a dimensionless quantity describing the third volume differential of the energy in units normalized to the volume and bulk modulus. In all cases we find this to be in the region 4–6, typical of experimental values. The fitting errors for this quantity are of order 25%, being especially unstable with respect to data points taken at high compression.

We also observe that there is some debate as to whether a Murnaghan fit is appropriate in these structures. Some of the calculated points are at unphysical compressions of up to 30%. Since compression is taken up by a combination of internal distortion and bond compression, the approximation that  $dB/dP$  is a constant throughout this huge pressure range is extremely doubtful.

The calculated valence charge densities for silicon and germanium in the BC8 and ST12 structures are shown in Fig. 6. Figures (a), (b), (d), and (e) represent the

valence charge density in a plane containing both *A* and *B* bonds for BC8 silicon and germanium.

### B. Carbon

The energy-vs-volume graph for carbon is shown in Fig. 3(c). It is immediately clear that the atomic volumes of all phases are rather similar, and therefore that BC8 is unlikely to be even a metastable phase. The energy difference is also very much greater than for silicon. These results for BC8 are in agreement with previous calculations,<sup>9</sup> where the rather surprising conclusion that BC8 may exist was drawn. In Fig. 7 the value of the BC8 internal parameter  $x$  is shown. It is clearly very different from Si and Ge, and consideration of the bond lengths shows that the *A* bond is much shorter than the *B* bonds.

All these results suggest that carbon is behaving very differently from the other materials, and the difference in bonding can be clearly seen in Fig. 8. Far from being

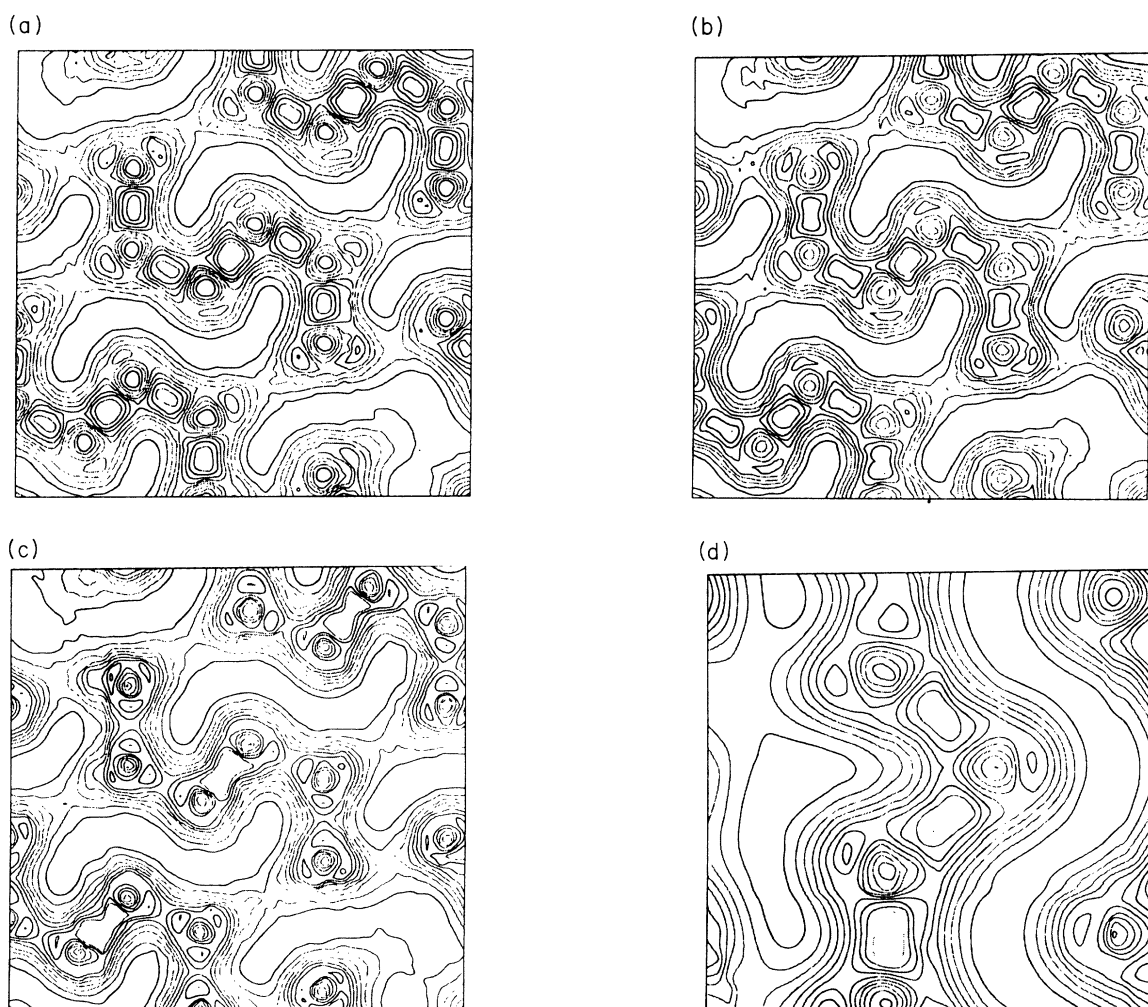


FIG. 6. Figures (a), (b), and (c) show the valence charge density for germanium, silicon, and carbon, respectively, in the BC8 structure. The plane shown is (110) which contains both *A* and *B* bonds. Figures (d), (e), and (f) show the valence charge densities for these elements in the ST12 structure. Figure (g) shows schematic representations of the atomic positions and bonding configurations of both the structures. Note that silicon and germanium appear to be covalently bonded in both structures, whereas carbon has a much reduced charge density between the weakly “bonded” atoms. This is also clearly evidenced in Fig. 9.

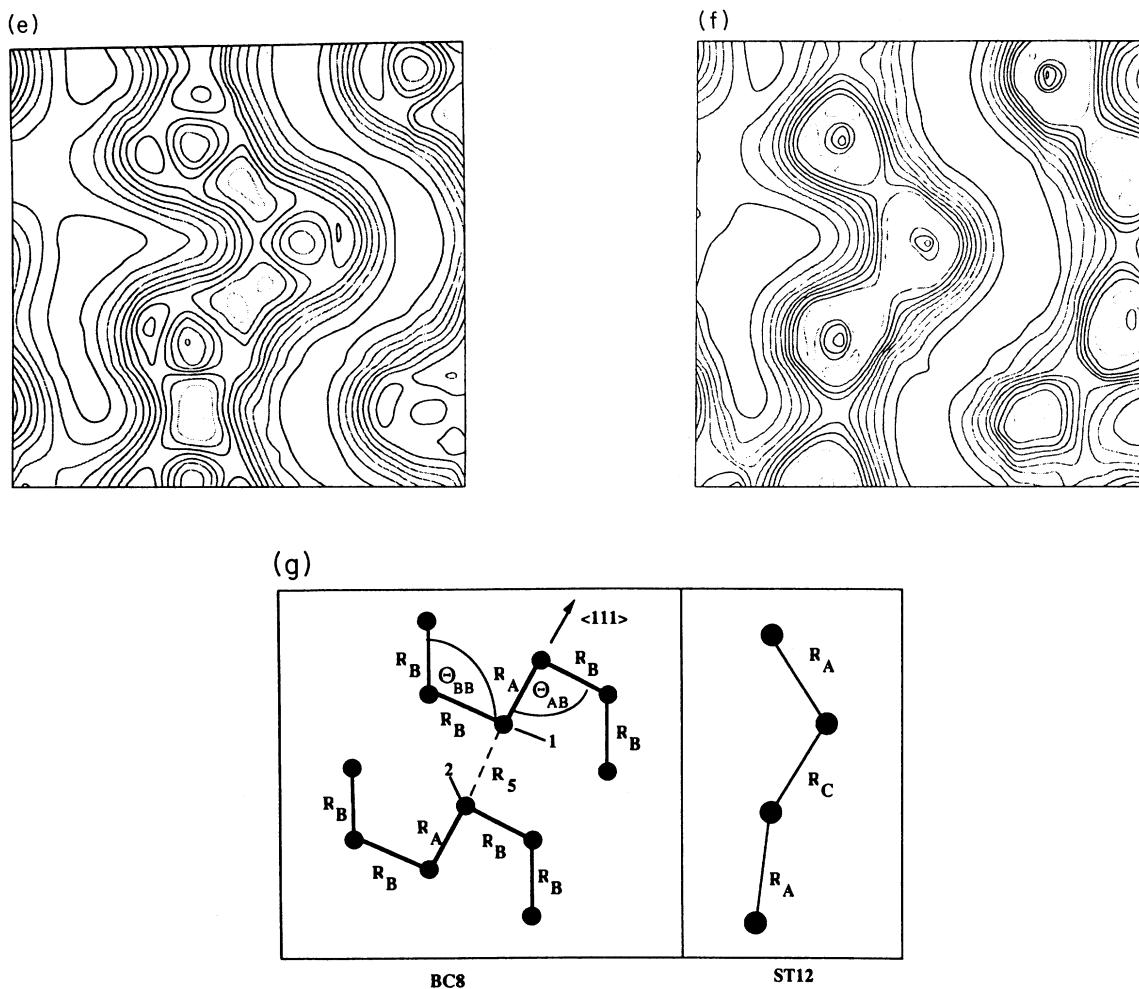


FIG. 6. (Continued).

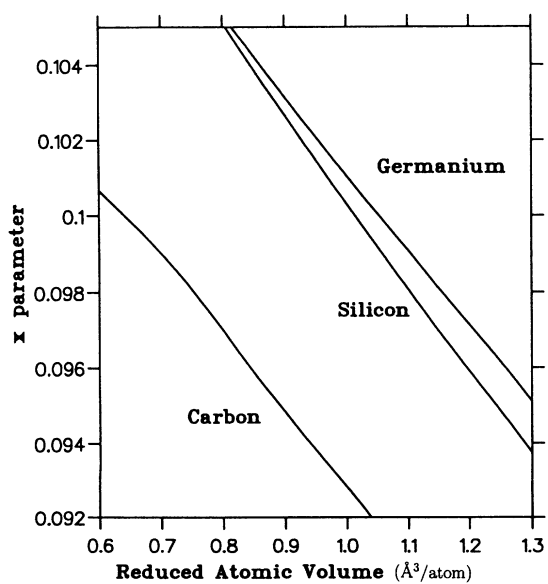


FIG. 7. Graph showing variation of BC8 internal parameter  $x$  as a function of normalized atomic volume in C, Si, and Ge.



FIG. 8. Three-dimensional representation of a valence-charge-density isosurface in BC8 carbon. The large black spheres represent the pseudopotential core radius around the atoms.

fourfold coordinated, the valence electrons are concentrated in one bond only, with the three *B* bonds much reduced.

To examine this more closely, we attempted to integrate the amount of charge in each bond. There is no unique way of doing this: our method consists of defining the bonds by the line joining the two atoms, and then associating with that bond the region of space closer to that bond's line than to any other bond's line. This construction produces space-filling polyhedra and ensures that the total integrated density is equal to the number of electrons. It has the drawback that purely spherical charge densities give the same number of electrons per bond as purely covalent ones, but in the current case we are assuming covalency, and studying whether the bonds are of similar order. In Figs. 9(a) and (b) the charge densities

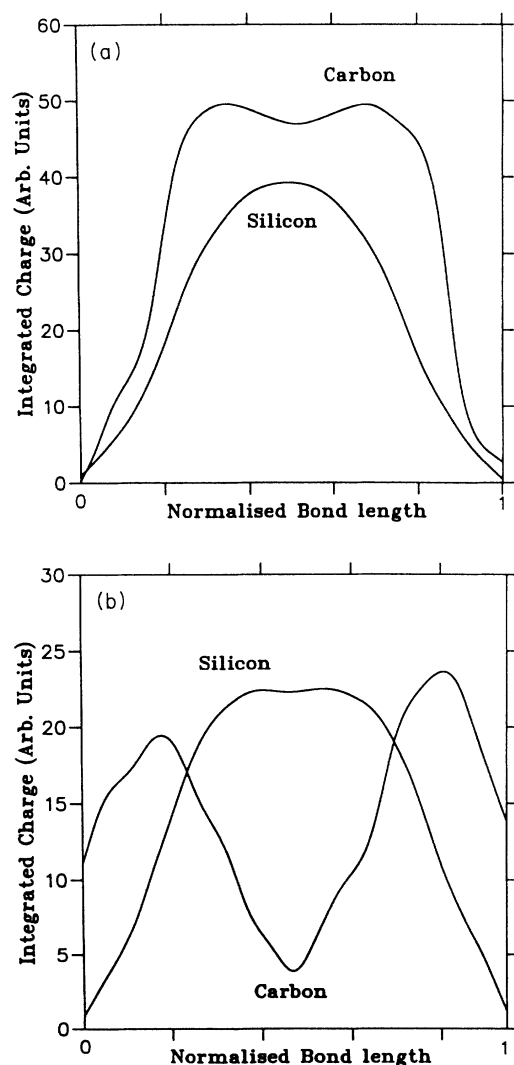


FIG. 9. Valence charge density for silicon and carbon in the BC8 structure along the (a) *A* bond and (b) *B* bond. The integrated charge in the carbon *A* bond is 2.6 electrons compared to 2.0 for that found in silicon and in ideal covalent bonding. The carbon *B* bond has a charge of only 1.8 electrons and a minimum at the bond center.

in slices of these polyhedra perpendicular to the bond direction along C-C bonds in the BC8 structure are compared to the corresponding bonds in silicon. The electron density in the Si bonds is localized between the atoms with a total charge of 2.0 electrons in each type of bond. This situation corresponds to completely covalent bonding in BC8 silicon. In carbon, however, it is evident that the *B* bonds are different in nature from those in BC8 silicon. The charge density has a minimum between the two *B*-bonded atoms, suggesting a much weaker bond. Integration over the charge density gives a total charge of only 1.8 electrons in the carbon *B* bonds. For the BC8-carbon *A* bond, the integrated charge is approximately 2.6 electrons. This suggests that BC8-carbon *A* bonds are stronger than single-bonded C-C. We attribute this to the formation of an unstable molecular crystal phase of carbon, with the fourfold-coordinated BC8 phase being still less stable.

The apparent metastable BC8 state in carbon arises from constraining the simulation to have certain symmetries. The Hellmann-Feynman forces must have the same symmetries as the ions, and our current method of minimization does break these symmetries. Consequently, although the BC8 phase is extremely unfavorable in carbon, the minimization routine finds the best compromise structure subject to those assumed symmetries, which turns out to be the molecular crystal.

There have been a number of previous calculations of BC8 carbon, limited by computing resources to much smaller cutoff energies. The results of these are rather similar to Fig. 3(c) but have been interpreted as generating a phase transition between diamond and BC8 at extremely high pressures (Biswas *et al.*<sup>9</sup> quote 1200 GPa, which is approximately the pressure found at the center of giant planets such as Jupiter). We do not observe this crossover, and moreover the evidence of our charge-density plot led us to suspect that BC8 may not even be metastable.

To test this latter hypothesis, we performed a calculation in which all the atoms were given a small random displacement from their equilibrium sites. From there, free relaxation under the Hellmann-Feynman forces restored the atoms to their BC8 symmetric positions. Thus the BC8 phase is at least metastable against any small atomic displacements.

For the ST12 structure of carbon, the equilibrium *c/a* ratio is 1.30 and the equilibrium atomic volume is slightly larger than that calculated for diamond. This suggests that, for carbon, unlike the other group-IV elements considered, the ST12 structure does not constitute a dense phase.

The calculated difference between diamond and BC8 silicon was found to be 0.11 eV/atom. This is in good agreement with the value reported by Biswas *et al.*<sup>9</sup> We find the difference in energy of the diamond and BC8 structure in carbon to be 0.7 eV/atom, which is also in good agreement with Biswas *et al.* In germanium the differences are very small, about 0.01 eV/atom. This distinct trend down the group can be understood as an increasing ease of distortion of *sp*<sup>3</sup> hybrids with principal quantum number.<sup>12</sup> Our results for the differences in en-

TABLE II. Differences in energies,  $\delta E$ , between the diamond and BC8 and ST12 structures. The units are eV/atom. Note that the difference in energy between the diamond and ST12 structures changes by nearly two orders of magnitude for the group-IV elements considered here.

$\delta E$	Carbon	Silicon	Germanium
$\delta_{BC8}$	0.5876	0.1100	0.0325
$\delta_{ST12}$	0.7634	0.1181	0.0147

ergy between diamond and the BC8 and ST12 structures are summarized in Table II.

### V. STRUCTURAL RESPONSE TO COMPRESSION

In both dense phases, as the volume is reduced the distortions of the tetrahedra increase. In the BC8 structure these distortions are uniquely described by the variation in the  $x$  parameter as described in Sec. III. For the BC8 structures of Si, Ge, and C the structural response to applied pressure is represented in Fig. 7, where the calculated variation in the free structural parameter  $x$  is shown. It is clear that both BC8-Si and BC8-Ge behave similarly under pressure as the equilibrium value of  $x$  and its slope are nearly equal in the two materials. For Si, the value of  $x$  which fully relaxes the structure is found to be  $x = 0.1001$  at the equilibrium lattice constant of 6.54 Å. The experimental value is reported to be  $x = 0.1003 \pm 0.0008$ . For fully relaxed BC8-Ge,  $x = 0.1013$ . In BC8-carbon, the equilibrium value of  $x = 0.0935$  is approximately 6% smaller than it is for Si or Ge.

Although plots of  $x$  give a complete representation of the data from our calculations, which are done at constant volume, it is more informative to examine the variation of bond lengths with pressure, and this is plotted in Fig. 10. Notice that under pressure  $x$  increases, which tends to compensate for decreasing  $a_0$  in  $R_A$ , but enhances the reduction in  $R_5$ . The effect on  $R_B$  is small ( $dR_B/dx = (8x - 1)a_0/R_B$ ) but gives rise to a small additional decrease in  $R_B$  with pressure, in addition to the reduction in  $a_0$ .

The effect of this compensation against decreasing  $R_A$  is that, whilst at ambient pressure the  $A$  bonds are shorter, as the pressure increases the  $B$  bond contracts until at  $x = (\sqrt{2} - 1)/4$  all bonds are the same length. There is no special symmetry associated with this coincidence, and the  $B$  bond length continues to contract. A qualitative explanation of this comes from the empirical model in Paper II.

Consideration of the differentials of expressions (4) and (5) makes it clear that  $\Theta_{AB}$  decreases with increasing  $x$  (pressure) while  $\Theta_{BB}$  increases. Thus pressure serves to increase the distortion of the tetrahedra: the price which must be paid for maintaining bond lengths. It is thus clear that the observation of increasing  $x$  with pressure means that the bond-stretching forces have a greater bearing on the structure than the bond-bending ones.

In ST12 the structure is only fully defined by four internal parameters. For this reason it is essential to relax

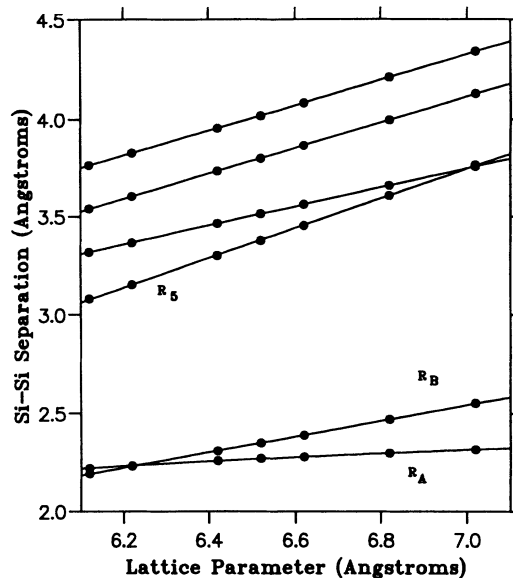


FIG. 10. Variation of bond lengths  $A$ ,  $B$  and the second neighbor with pressure for BC8 silicon. The graph for germanium is similar. It is evident from the figure that the nearest-nonbonded-neighbor distance ( $R_5$ ) is most sensitive to isotropic compression. The second nearest appears to be least sensitive. Note that the  $A$  bond changes by less than 0.1 Å over the entire range of compression shown. This insensitivity results in a bond length crossover point at a lattice parameter of approximately 6.25 Å.

the structure under the Hellmann-Feynman forces, and thus study of ST12 is ideal for the plane-wave method. The relationships between these internal parameters and the bond lengths and bond angles are complex, and for clarity we consider only the latter quantities. The evolution of the internal structure under pressure is described by Fig. 11, which depicts the change of the three different bond lengths under pressure.

Following the notation of Kasper and Richards<sup>37</sup> for ST12-Ge, the four atomic positional parameters are

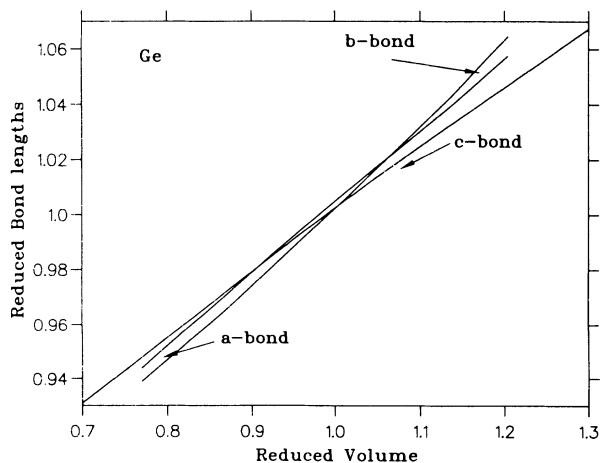


FIG. 11. Variation of the three different bond lengths in ST12 germanium with volume.

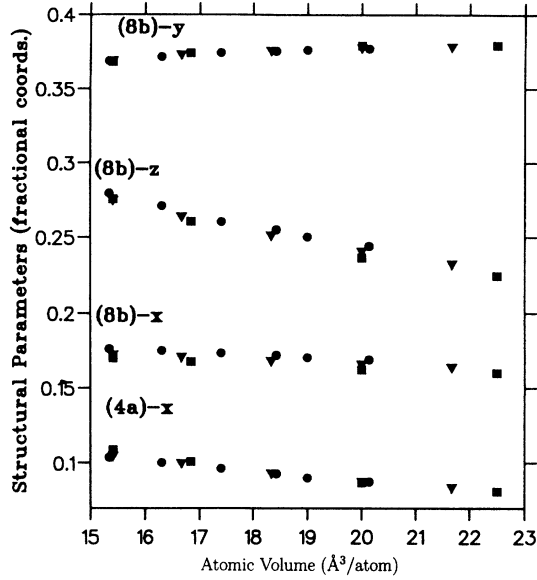


FIG. 12. The relaxed ST12 structural parameters for germanium plotted against volume. The circles, squares, and triangles represent axial ratios of 1.25, 1.30, and 1.35, respectively.

shown for axial ratios of 1.2, 1.25, and 1.3 in Fig. 12. It is evident from the figure that the  $z$  parameter for the 8(b) site has the strongest dependence on isotropic compression of the unit cell, and that the positional parameters are not greatly affected by changes in axial ratio over the range considered here. The ST12-Ge positional parameters near the equilibrium volume and  $c/a$  ratio may be found from Table II. The calculated value of  $x$  for the 4(a) sites is 0.0882 compared to 0.0912 found experimentally. The calculated  $x$ ,  $y$ , and  $z$  values for the 8(b) sites are  $x = 0.1693$ ,  $y = 0.3771$ , and  $z = 0.2454$ . The corresponding experimental values at ambient pressure are  $x = 0.1730$ ,  $y = 0.3784$ , and  $z = 0.2486$ . The agreement is

encouraging and suggests that future experiments using recent advances in angle-dispersive powder diffraction<sup>40</sup> to determine the pressure dependence of this structure would be of great value.

As in BC8, the ST12 internal parameters vary with pressure to maintain the bond lengths at the expense of further distorting the bond angles. Figure 11 shows that for a constant  $c/a$  ratio the bond lengths are reduced more slowly as a function of volume than the unit cell parameters. In practice the  $c/a$  ratio also changes under pressure in such a way as to reduce the changes in bond lengths. The fully relaxed unit-cell dimensions and atomic positions in fractional coordinates for silicon, germanium, and carbon in the BC8 and ST12 structures are given in Tables III and IV.

## VI. THE NATURE OF THE BONDING

BC8 Si has a small Fermi surface and thus electronically can be regarded as a semimetal. Its fourfold coordination and brittleness suggest that it is predominantly held together by directional covalent bonds. To resolve this apparent contradiction we have examined the valence charge density within BC8 and ST12. Figure 13 shows an electron-density isosurface in ST12 silicon. It bears an uncanny resemblance to a ball-and-stick model of the structure, showing clearly that the electron density is concentrated into four “bonds” emanating from each atom—the covalent picture.

This covalency is illustrated even more clearly in Fig. 6, which shows the valence charge density in the (110) plane of BC8. Along the [111] direction are atoms separated by  $2\sqrt{3}xa_0$  and  $\sqrt{3}(\frac{1}{2}-2x)a_0$  alternately. Although these distances are similar, it can very clearly be seen that the slightly closer pairs are bonded, while the more distant pairs are not. This effect cannot be seen in diamond because there are no “second neighbors” as close. An interesting aspect of this structure is that if the topology of the crystal is defined by bonds, it requires six steps to

TABLE III. Fully relaxed positions (in fractional coordinates) of the atoms of BC8 silicon, germanium, and carbon near the relaxed unit cell volume. Note that the simple cubic representation of the BC8 structure is used.

Silicon			Germanium			Carbon		
$x$	$y$	$z$	$x$	$y$	$z$	$x$	$y$	$z$
0.1001	0.1001	0.1001	0.0994	0.0995	0.0995	0.0935	0.0934	0.0935
0.8998	0.8998	0.8998	0.9004	0.9005	0.9005	0.9064	0.9063	0.9064
0.3997	0.8998	0.6001	0.4004	0.9005	0.5995	0.4064	0.9063	0.5936
0.6001	0.1001	0.3998	0.5994	0.0995	0.4005	0.5935	0.0934	0.4064
0.8998	0.6002	0.3998	0.9004	0.5995	0.4005	0.9064	0.5934	0.4064
0.1001	0.3998	0.6001	0.0994	0.4005	0.5995	0.0936	0.4063	0.5936
0.6001	0.3998	0.8998	0.5994	0.4005	0.9005	0.5936	0.4063	0.9064
0.3997	0.6002	0.1001	0.4004	0.5995	0.0995	0.4064	0.5934	0.0935
0.6001	0.6001	0.6001	0.5994	0.5995	0.5995	0.5936	0.5934	0.5936
0.3998	0.3998	0.3997	0.4004	0.4005	0.4005	0.4064	0.4063	0.4064
0.8997	0.3998	0.1001	0.9004	0.4005	0.0995	0.9064	0.4063	0.0936
0.1001	0.6001	0.8998	0.0994	0.5995	0.9005	0.0935	0.5934	0.9064
0.3998	0.1002	0.8998	0.4004	0.0995	0.9005	0.4064	0.0934	0.9064
0.6001	0.8998	0.1001	0.5994	0.9005	0.0995	0.5935	0.9063	0.0935
0.1001	0.8998	0.3998	0.0994	0.9005	0.4005	0.0935	0.9063	0.4064
0.8997	0.1002	0.6001	0.9004	0.0995	0.5995	0.9064	0.0934	0.5936

TABLE IV. Fully relaxed positions (in fractional coordinates) of the atoms of ST12 silicon, germanium, and carbon near the relaxed unit cell volume.

Silicon			Germanium			Carbon		
$x$	$y$	$z$	$x$	$y$	$z$	$x$	$y$	$z$
0.1752	0.3792	0.2742	0.1693	0.3771	0.2454	0.1641	0.3803	0.2143
0.8247	0.6207	0.7472	0.8305	0.6228	0.7454	0.8360	0.6195	0.7143
0.1208	0.6750	0.9973	0.1227	0.6694	0.9953	0.1197	0.6639	0.9644
0.8792	0.3248	0.4973	0.8771	0.3305	0.4954	0.8804	0.3359	0.4644
0.3792	0.1752	0.7528	0.3771	0.1693	0.7546	0.3804	0.1639	0.7856
0.6207	0.8247	0.2527	0.6228	0.8305	0.2546	0.6197	0.8359	0.2856
0.3248	0.8791	0.5027	0.3305	0.8771	0.5046	0.3360	0.8803	0.5356
0.6751	0.1208	0.0027	0.6694	0.1228	0.0046	0.6641	0.1195	0.0356
0.0849	0.0849	0.0000	0.0882	0.0882	0.0000	0.0743	0.0742	0.0000
0.9151	0.9151	0.5000	0.9117	0.9117	0.5000	0.9258	0.9256	0.5000
0.4151	0.5848	0.7500	0.4116	0.5882	0.7500	0.4258	0.5742	0.7500
0.5849	0.4151	0.2500	0.5882	0.4117	0.2500	0.5743	0.4256	0.2500

get from an atom to its “second neighbor,” and there is only one such second neighbor per atom. Under pressure the increase in  $x$  has the effect of pushing these second neighbors together, but there is still no increase in the charge-density between the atoms.

We therefore deduce that while the electronic properties of BC8 are dominated by its small Fermi surface, and hence it is regarded as a semimetal, the cohesion is dominated by covalent bonding of each atom to four neighbors. This observation has been used in constructing a simple empirical model for silicon, which also seems to apply to structural features of the metallic  $\beta$ -Sn phase. Calculations using the empirical model are presented in Paper II. ST12 is a semiconducting phase, and again the charge-density plots suggest that a covalent picture for the bonding is appropriate.

## VII. TRENDS

It is now possible to make some comment about the trends in behavior down group IV. In Si, Ge, and Sn

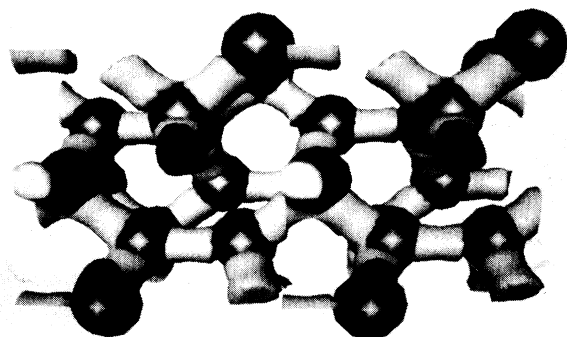


FIG. 13. Three-dimensional representation of a valence-charge-density isosurface in ST12 silicon. The large black spheres represent the pseudopotential core radius around the atoms. The equivalent plot for germanium is similar.

the stable phase at low pressure and temperature is diamond whilst in C this phase is metastable with respect to graphite. Under pressure the transformation to the metallic  $\beta$ -Sn structure occurs at progressively lower pressures in Si-Ge-Sn (in tin itself, this transition occurs at ambient pressure due to temperature alone). Likewise, metastable phases exist which have intermediate density and maintain fourfold coordination. These are easier to form as one goes down group IV, apparently because bond bending is easier for  $sp^3$  hybrids with larger  $n$  (and therefore smaller overlap under distortions). These concepts are used in the development of empirical potentials, and are developed further in the related paper. Carbon is different. Not only does it exhibit the graphite phase under ambient pressure but it cannot form a metastable phase with BC8 or ST12 symmetry without a significant departure from fourfold coordination.

## VIII. CONCLUSIONS

We have performed total-energy pseudopotential calculations on high-density phases of the group-IV elements Si, Ge, and C. Using the density-functional molecular-dynamics method of Car and Parrinello, the fully relaxed BC8 and ST12 structures of these elements have been determined via relaxation under the influence of the Hellmann-Feynman forces, and they are found to be in good agreement with available diffraction data. The structural response to compression has also been investigated. Using these results it will be possible to calculate pressure-induced effects on the optical properties of these materials. This will be the subject of a future paper.<sup>11</sup>

This method has also allowed us to determine lattice parameters, bulk moduli, and behavior of the internal structure under pressure. These are found to be in very good agreement with the available experimental data, although as usual with LDA the structures tend to be overbound slightly. This overbinding means that the lattice parameters are invariably too small by about 2%, and the binding energy is too large by about 15%. It is well established, however, that the energy differences between

various structures are well reproduced by LDA.

In silicon our predictions confirm that at low temperature the metastable phase is BC8. *Ab initio* calculation of the entropy at high temperature is currently impractical, so we have carried out this simulation using an empirical potential in Paper II.

In germanium the energies of all phases are similar, reflecting the ease with which the germanium bonds can be distorted, and that cohesive energy is dominated by the requirement of fourfold coordination. We found that the internal parameters in both BC8 and ST12 germanium adjust to maintain all bondlengths to be similar. The energy difference between ST12 and diamond was much smaller than that of carbon or silicon. Convergence of this difference required the use of a denser *k*-point set for band-structure sampling.

Although the germanium energy differences are close to the accuracy of our programs, we predict that within a range of pressures ST12 will actually be the stable phase of germanium. It would be interesting to attempt to verify this experimentally; although the large kinetic barrier makes the direct transition between diamond and ST12 impossible, ST12 can be made via the  $\beta$ -Sn phase. BC8 is found to be close but slightly higher in energy.

In carbon we predict that diamond will be completely stable with respect to BC8 or ST12 at all reasonable pressures, and that those phases, while not mechanically unstable, have fundamentally different bonding from that in Si and Ge.

## ACKNOWLEDGMENTS

The authors wish to acknowledge the valuable assistance received from J. S. Lin and M. H. Lee with generating the pseudopotentials and J. McLean, R. Smith, and S. Dickie for help with data analysis. We are indebted to Edinburgh Parallel Computing Centre for use of their graphics facilities, DEC for loan of an Alphavx work station during  $\beta$  testing, and Edinburgh University Computing Service for allowing us to carry out this work as a part of this test. We would also like to thank the other members of the "U.K. Grand Challenge in Condensed Matter" for useful discussions and Professor R. J. Nelmes for making his results in germanium available to us prior to publication. G.J.A. would like to thank BP and the Royal Society of Edinburgh for support. J.C. and S.J.C. thank the SERC for support.

\*Present address: Cavendish Laboratory, University of Cambridge, Madingley Road, Cambridge CB3 08E, United Kingdom.

<sup>1</sup>S.B. Quadrie, E.F. Skelton, and A.W. Webb, *J. Appl. Phys.* **54**, 3609 (1983).

<sup>2</sup>Y.K. Vohra, K.E. Brister, S. Desgreniers, A.L. Ruoff, K.J. Chang, and M.L. Cohen, *Phys. Rev. Lett.* **56**, 1944 (1986).

<sup>3</sup>F.B. Bundy and J.S. Kasper, *Science* **139**, 340 (1963).

<sup>4</sup>A. Gruttner, R. Nesper, and H.G. von Schnering, *Angew. Chem.* **94**, 933 (1982).

<sup>5</sup>J. Pethica (private communication).

<sup>6</sup>M.T. Yin, *Phys. Rev. B* **30**, 1773 (1984).

<sup>7</sup>M.T. Yin and M.L. Cohen, *Phys. Rev. Lett.* **50**, 1172 (1983).

<sup>8</sup>M. Needels, M.C. Payne, and J.D. Joannopolis, *Phys. Rev. B* **38**, 5543 (1988).

<sup>9</sup>R. Biswas, R.M. Martin, R.J. Needs, and O.H. Nielson, *Phys. Rev. B* **35**, 9559 (1987).

<sup>10</sup>J.D. Joannopoulos and Marvin L. Cohen, *Phys. Rev. B* **8**, 2733 (1973).

<sup>11</sup>S.J. Clark, J. Crain, and G.J. Ackland (unpublished).

<sup>12</sup>S.J. Clark, G.J. Ackland, and J. Crain, following paper, *Phys. Rev. B* **49**, 5341 (1994).

<sup>13</sup>J.Z. Hu, L.D. Merkle, C.S. Menoni, and I.L. Spain, *Phys. Rev. B* **34**, 4679 (1986).

<sup>14</sup>Y.X. Zhao, F. Beuhler, J.R. Sites, and I.L. Spain, *Solid State Commun.* **59**, 679 (1986).

<sup>15</sup>P.D. Hatton, J. Crain, and R.O. Piltz (unpublished).

<sup>16</sup>J.M. Besson, E.H. Mokhtari, J. Gonzales, and G. Weill, *Phys. Rev. Lett.* **59**, 473 (1987).

<sup>17</sup>C.S. Menoni, J.Z. Hu, and I.L. Spain, *Phys. Rev. B* **34**, 362 (1986).

<sup>18</sup>C.H. Bates, F. Dache, and R. Roy, *Science* **147**, 860 (1965).

<sup>19</sup>R.J. Nelmes and M.I. McMahon (unpublished).

<sup>20</sup>M. Imai, T. Mitamura, K. Yaoita, and K. Tsuji, *J. Non-Cryst. Solids* **150**, 49 (1992).

<sup>21</sup>S. Minomura and H. G. Drickamer, *Phys. Chem. Solids* **23**, 451 (1962).

<sup>22</sup>R.H. Wentorf and J.S. Kasper, *Science* **338**, 139 (1964).

<sup>23</sup>J.S. Kasper and S.M. Richards, *Acta. Cryst.* **77**, 752 (1964).

<sup>24</sup>J.Z. Hu and I.L. Spain, *Solid State Commun.* **51**, 263 (1984).

<sup>25</sup>J.Z. Hu, L.D. Merkle, C.S. Menoni, and I.L. Spain, *Phys. Rev. B* **34**, 4679 (1986).

<sup>26</sup>G. Weill, J.L. Mansot, G. Sagon, C. Carlone, and J.M. Besson, *Semicond. Sci. Tech.* **4**, 280 (1989).

<sup>27</sup>R. Biswas, R.M. Martin, R.J. Needs, and O.H. Nielson, *Phys. Rev. B*, **30**, 3210 (1984).

<sup>28</sup>R. Car and M. Parrinello, *Phys. Rev. Lett.* **55**, 2471 (1985).

<sup>29</sup>M.C. Payne, M.P. Teter, D.C. Allan, T.A. Arias, and J.D. Joannopolous, *Rev. Mod. Phys.* **64**, 1045 (1992).

<sup>30</sup>W. Kohn and L.J. Sham, *Phys. Rev.* **140**, 1133A (1965).

<sup>31</sup>J.P. Perdew and A. Zunger, *Phys. Rev. B* **23**, 5048 (1981).

<sup>32</sup>D.M. Ceperley and B.J. Alder, *Phys. Rev. Lett.* **45**, 566 (1980).

<sup>33</sup>L. Kleinman and D.M. Bylander, *Phys. Rev. Lett.* **48**, 1425 (1982).

<sup>34</sup>G.P. Kerker, *J. Phys. C* **13**, L189 (1980).

<sup>35</sup>P. Pulay, *Mol. Phys.* **17**, 197 (1969).

<sup>36</sup>H.J. Monkhorst and J.D. Pack, *Phys. Rev. B* **13**, 5188 (1976).

<sup>37</sup>J.S. Kasper and S.M. Richards, *Acta. Cryst.* **17**, 752 (1964).

<sup>38</sup>L.L. Boyer, B. Kaxiras, J.L. Feldman, J.Q. Broughton, and M.J. Mehl, *Phys. Rev. Lett.* **67**, 715 (1991).

<sup>39</sup>E. Kaxiras and L.L. Boyer, *Model. Simul. Mater. Sci. Eng.* **1**, 91 (1992).

<sup>40</sup>R.J. Nelmes, P.D. Hatton, M.I. McMahon, R.O. Piltz, J. Crain, R.J. Cernik, and G. Bushnell-Wye, *Rev. Sci. Instrum.* **63**, 700 (1992).

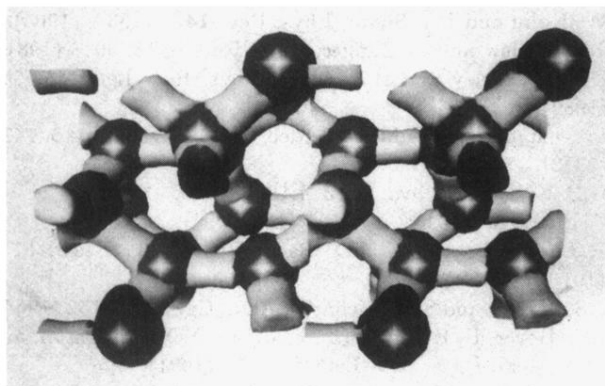


FIG. 13. Three-dimensional representation of a valence-charge-density isosurface in ST12 silicon. The large black spheres represent the pseudopotential core radius around the atoms. The equivalent plot for germanium is similar.

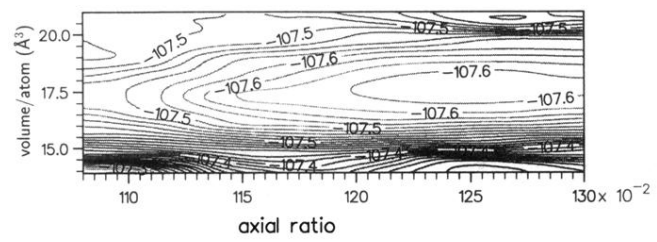


FIG. 4. Contour plot of cohesive energy against  $c/a$  ratio and atomic volume for ST12 structure in silicon.

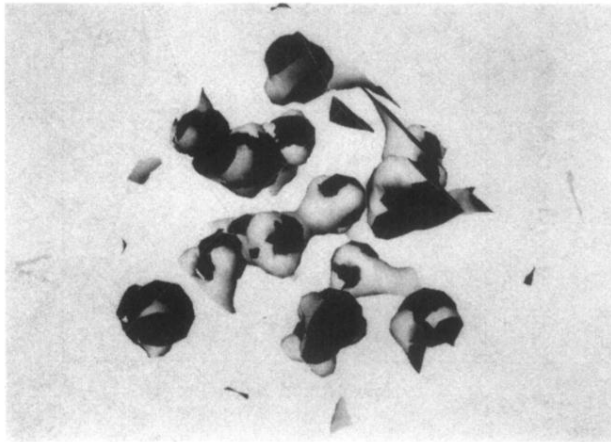


FIG. 8. Three-dimensional representation of a valence-charge-density isosurface in BC8 carbon. The large black spheres represent the pseudopotential core radius around the atoms.